

DOI: 10.1002/adma.200602377

Visible-Light Photocatalytic Properties of Weak Magnetic BiFeO₃ Nanoparticles**

By Feng Gao, Xinyi Chen, Kuibo Yin, Shuai Dong, Zhifeng Ren, Fang Yuan, Tao Yu, Zhigang Zou, and Jun-Ming Liu*

In recent years, multiferroics, showing the coexistence of magnetic and ferroelectric orders in a certain range of temperature, have attracted a great deal of attention due to the fascinating fundamental physics and potential applications for novel magnetoelectric devices.^[1] Among all multiferroic materials studied so far, perovskite-type BiFeO₃ (BFO) is known to be one of the several compounds that exhibit ferromagnetism (FM) at room temperature (RT), with high ferroelectric (FE) Curie point ($T_C \sim 1103$ K)^[2] and G-type antiferromagnetic (AFM) Néel point ($T_N \sim 647$ K).^[3] In addition to the potential magnetoelectric applications, BFO might find applications as photocatalytic materials due to its small bandgap. This small bandgap also allows carrier excitation in BFO with commercially available femtosecond laser pulses, hence enables us to develop ferroelectric ultrafast optoelectronic devices as widely demonstrated in semiconductors.^[4] In fact, regarding the photocatalytic property of BFO, it was demonstrated that SrTiO₃ coated BFO nanoparticles can produce H₂ under the irradiation of visible light, whereas pure SrTiO₃ only responded to UV irradiation.^[5] More recently, we have reported the oxidation (oxygen generation) ability of BFO nanowires, suggesting that BFO nanostructures might be useful for photocatalytic decomposition of organic contaminants.^[6]

Although weak ferromagnetic (FM) order was observed in BFO films at RT,^[7] different from the AFM magnetic nature of BFO ceramics,^[8] the origin in films is not fully understood.^[7,9] Recently, Bea et al. attributed the magnetic moment in BFO films to the extra phase like γ -Fe₂O₃ and argued that BFO phase has a very small magnetic moment if any.^[10] We reported weak FM order in BFO nanowires and suggested that the size effect in nanostructures like films and nanowires might be responsible for the FM property.^[6] In this communication, we report the synthesis of BFO nanoparticles by a sol-gel technique and its photocatalytic and magnetic properties.

Figure 1a presents the XRD pattern of the nanoparticles prepared under the optimal conditions (calcined at 500 °C for 2 h, the detail of preparation is described in the Experimental Section). It is revealed that the BFO nanoparticles are highly crystallized and exhibit a single-phase perovskite structure. Non-perovskite phases such as Bi₂Fe₄O₉ and Bi₂O₃/Fe₂O₃ are not detected in XRD spectra. The obvious peak-splitting shows that the nanoparticles are rhombohedral, consistent with the structure of BFO ceramics,^[8] but different from the tetragonal structure of BFO films.^[9] Figure 1b shows the XRD spectra of the sample after degradation experiments in methyl orange (MO), which are described later in details.

The typical scanning electron microscopy (SEM) image of the BFO powders is shown in Figure 2a, where the inset is a representative transmission electron microscopy (TEM) image. These nanopowders consist of roughly spherical and well-dispersed particles ranging from 80 to 120 nm. Figure 2b

[*] Prof. J.-M. Liu, F. Gao, X. Y. Chen, K. B. Yin, S. Dong, F. Yuan, Prof. T. Yu, Prof. Z. G. Zou
Laboratory of Solid State Microstructures
Nanjing University
Nanjing 210093 (P.R. China)
E-mail: liujm@nju.edu.cn
Prof. J.-M. Liu
International Center for Materials Physics
Chinese Academy of Sciences
Shenyang 110015 (P.R. China)
X. Y. Chen, Prof. T. Yu, Prof. Z. G. Zou
Eco-Materials and Renewable Energy Research Center
Nanjing University
Nanjing 210093 (P.R. China)
Prof. Z. F. Ren
Department of Physics
Boston College
Chestnut Hill, MA 02467 (USA)

[**] This work was supported by the National Key Projects for Basic Research of China (2002CB613303, 2006CB921802) and the National Natural Science Foundation of China (50332020, 50528203, 20373025, and 20528302).

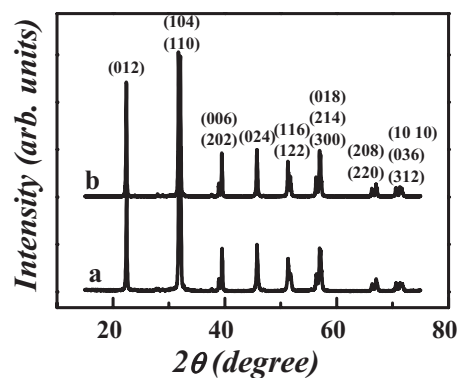


Figure 1. XRD patterns of the BFO nanoparticles: a) synthesized under the optimal conditions (500 °C for 2 h); b) after the degradation experiment in methyl orange.

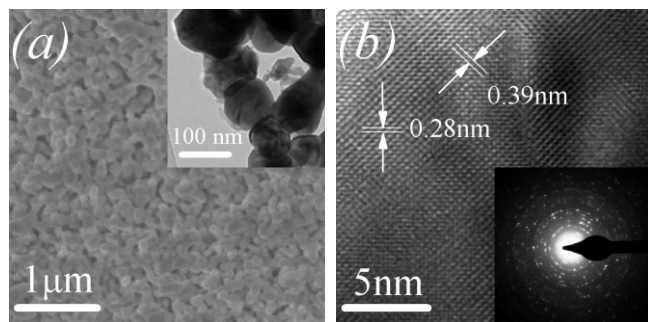


Figure 2. a) SEM image of BFO nanoparticles with the TEM image as the inset; b) HRTEM image of the nanoparticles with the SAED pattern as the inset.

shows the high-resolution TEM (HRTEM) image of the BFO nanoparticle as well as the selected area electron diffraction pattern (SAED) (inset). Both of them confirm that the BFO nanoparticles are well crystallized with a single-phase perovskite structure. In addition, X-ray energy dispersive spectroscopy (EDS) attached to TEM was used to measure the Bi:Fe ratio in our sample. The quantitative analysis was averaged over five different samplings,^[11] revealing that the ratio of Bi to Fe is about 1:1 within the instrumental accuracy. This result was confirmed by inductively coupled plasma resonance (ICP) spectroscopy measurement, which showed that the ratio of Bi to Fe was 0.99:1.00.

Before the photocatalytic activity characterization, it is important to study the optical absorption of the as-prepared BFO nanoparticles because the UV-vis absorption edge is relevant to the energy band of semiconductor catalyst. Figure 3a shows the absorption spectra of the as-prepared BFO sample transformed from the diffuse reflection spectra according to the Kubelka–Munk (K–M) theory.^[12] The absorption cut-off wavelength of the as-prepared BFO sample is about 565 nm, suggesting that the present material can absorb visible light in the wavelength range of 400–565 nm. The energy bandgap of BFO nanoparticles could be estimated from the tangent line in the plot of the square root of Kubelka–Munk functions $F(R)$ against photon energy,^[13] as shown in Figure 3b. The tangent line, which is extrapolated to $(F(R))^{1/2} = 0$, indicates the bandgap is 2.18 eV. Such an energy bandgap is smaller compared with the bandgap of BFO films (2.5 eV),^[4] possibly due to the small thickness of the thin film sample. The smaller bandgap of BFO nanoparticles indicates a possibility of utilizing more visible light for photocatalysis.

The photocatalytic activity of BFO nanoparticles for MO degradation is shown in Figure 3c. As a typical organic contaminant, MO is stable under UV-vis irradiation if there is no photocatalyst involved. For example, after 15 h UV-vis irradiation without BFO nanoparticles, the degradation rate of MO was less than 3%. However, with BFO nanoparticles as photocatalysts, more than 90% of MO was decolorized after 8 h under UV-vis irradiation. After putting a filter glass to cut off the UV light (less than 420 nm), more than 90% of MO was decolorized after 16 h, showing efficient photocatalytic

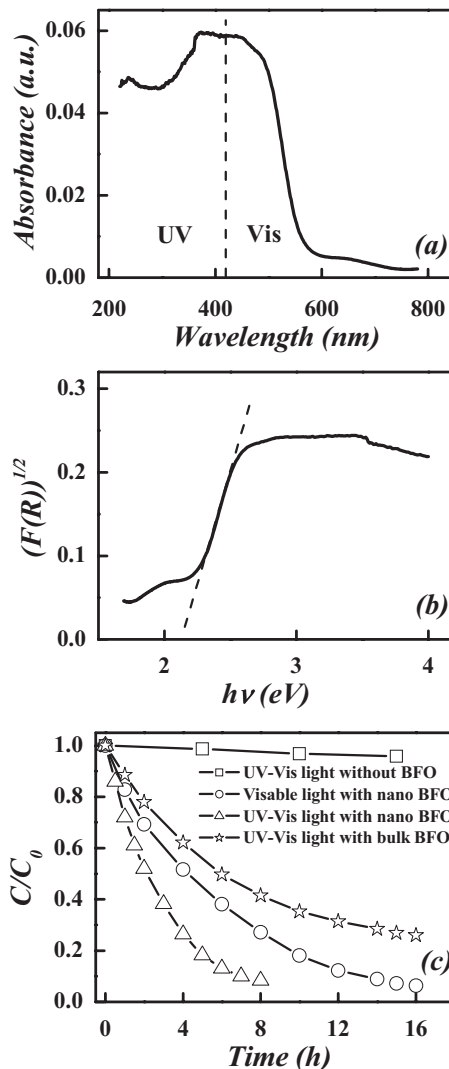


Figure 3. a) UV-vis diffuse reflectance spectrum of the BFO nanoparticles, where the dot line is the division between UV and visible light; b) the square root of Kubelka–Munk functions $F(R)$ versus photon energy, where the dot line is tangent of the linear part; c) photocatalysis of BFO nanoparticles and bulk on degradation of methyl orange under UV-vis light irradiation and visible light irradiation.

activity of BFO nanoparticles under visible light irradiation. Compared with the normal photocatalyst TiO_2 , which only has response to UV irradiation, BFO nanoparticles show their obvious advantage making use of the visible light. We also performed the degradation experiment on bulk BFO, which was prepared by the rapid liquid phase sintering technique developed in our laboratory.^[1,14] After 16 h UV-vis irradiation with bulk BFO, the MO degradation rate was saturated to about 70%, which was significantly less efficient than when BFO nanoparticles was used under the same condition.

It is well known that the surface area of a catalyst greatly affects its catalytic activity.^[15] The BET (Brunauer–Emmett–Teller) measurement showed that the surface area of the BFO nanoparticles was $8.3 \text{ m}^2 \text{ g}^{-1}$ while that of bulky ceramic BFO

powder was $1.2 \text{ m}^2 \text{ g}^{-1}$. Therefore, the significantly higher surface area of the BFO nanoparticles might be responsible for the higher efficiency. In addition, it is highly possible that MO can be degraded in shorter time by preparing photocatalyst BFO nanoparticles with smaller diameters (less than 80 nm) resulting in even higher surface area, which is being pursued.

From the application point of view, the stability of a photocatalyst is important. As an example, doped TiO_2 photocatalysts are not stable though doping could possibly make TiO_2 respond to visible light.^[16] In the case of BFO nanoparticles, the crystal structure of the BFO nanoparticles was very stable, as demonstrated by XRD spectra after the reaction with MO. As shown in Figure 1b, the crystal structure of the photocatalyst did not change after the photocatalytic reaction. The stability of BFO nanoparticle photocatalyst was further examined by investigating the pH value after the reaction. Each sample solution showed a pH value of 6.5–7.0, as steady as the photocatalysis on TiO_2 .^[17]

It was suggested that the size effect of BFO nanostructures might be responsible for the magnetic ordering by comparing the magnetic property of BFO films with that of BFO nanowires.^[6] In this communication, we investigated the magnetic ordering of the BFO nanoparticles. As shown in Figure 4, weak FM order with a saturated M of about $0.06 \mu_{\text{B}}/\text{Fe}$ is observed for the BFO nanoparticles at 300 K, which is different from the linear M – H behavior in bulk BFO.^[8] The partially enlarged M – H curve is shown in the inset, which reveals that the coercive field of the BFO nanoparticles is quite small (~ 100 Oe). It is necessary to point out that the saturated M in BFO films and nanowires are $0.04 \mu_{\text{B}}/\text{Fe}$ and $0.03 \mu_{\text{B}}/\text{Fe}$, respectively,^[6,7] comparable with the results in nanoparticles. In addition, the coercive fields of both the BFO films and nanowires are also quite small,^[6,7] also similar to that of the nanoparticles. Therefore, it is reasonable to say that there is similarity among BFO nanostructures (including films, nanowires and nanoparticles). It is such similarity that makes the magnetization of nanosized BFO different from that of bulk BFO. We suggest that the possible similarity lies in the nano-dimension of BFO films, nanowires and nanoparticles. It is well

known that the wavelength of the incommensurate cycloid spin structure in bulk BFO is 62 nm ^[18] and the scale of nanosized BFO is comparable with this wavelength. One may argue that the cycloid structure in bulk BFO is partially destroyed in the BFO nanostructures, which leads to the weak FM behaviors at RT. In fact, recent density functional calculations give a macroscopic M of about $0.05 \mu_{\text{B}}/\text{Fe}$,^[19] in good agreement with our experimental observation.

In summary, we have synthesized BFO nanoparticles ranging from 80 to 120 nm by a simple sol-gel method. The polycrystalline nanoparticles are single-phase with perovskite structure. Although both BFO bulk and nanoparticles demonstrate the photocatalytic ability to decompose methyl orange (a typical organic contaminant) under UV-vis light irradiation, the degradation with BFO nanoparticles is significantly more efficient than that of bulk BFO due to the higher surface area of nanosized BFO. Because of the small bandgap, BFO nanoparticles show significant degradation ability under visible light irradiation. In addition, weak ferromagnetism of the BFO nanoparticles is observed at RT, possibly due to the nanosize, which is different from the magnetic property of bulk BFO.

Experimental

Synthesis: Bismuth nitrate ($\text{Bi}(\text{NO}_3)_3 \cdot 5\text{H}_2\text{O}$) and iron nitrate ($\text{Fe}(\text{NO}_3)_3 \cdot 9\text{H}_2\text{O}$) in stoichiometric proportions (1:1 molar ratio) were dissolved in 2-methoxyethanol ($\text{C}_3\text{H}_8\text{O}_2$). The solution was adjusted to a pH value of 4–5 by adding nitric acid. Then citric acid in 1:1 molar ratio with respect to the metal nitrates was added to the solution as a complexant, followed by polyethylene glycol as a dispersant. The mixture was stirred for about half an hour at 50°C to obtain the sol, which was then kept at 80°C for 4 days to form the dried gel powder. The final powder was calcined at different temperatures of 400 – 700°C for different times of 1–3 h in air. The optimal calcining temperature and time for perovskite-type BFO nanoparticles are 500°C and 2 h, respectively.

Characterization: The structure and morphology of the BFO nanoparticles were investigated by X-ray diffraction (XRD), scanning electron microscopy (SEM) and transmission electron microscopy (TEM). The cationic stoichiometry of our sample was determined by inductively coupled plasma resonance (ICP). The UV-vis absorption spectra were measured on a UV-vis spectrophotometer. The photocatalytic activity of the BFO nanoparticles for decomposition of methyl orange (MO) was evaluated under irradiation of a 300 W Xe lamp at the natural pH value. The initial concentration of MO was 15 mg L^{-1} with a catalyst loading of 30 mmol L^{-1} . After the elapse of 0.5 or 1 h, a small quantity of the solution was taken, and the concentration of MO was determined by measuring the value at approximately 464 nm using a UV-vis spectrophotometer. Each time before the absorption measurement, the sample solution was centrifuged at $3000 \text{ rpm min}^{-1}$ for 10 min in order to separate the catalyst particles from the solution. The absorption was converted to the MO concentration referring to a standard curve showing a linear behavior between the concentration and the absorption at this wavelength. For the magnetic measurements carried out using a superconducting quantum interference device (SQUID) magnetometer, the BFO particles were pressed into a disk.

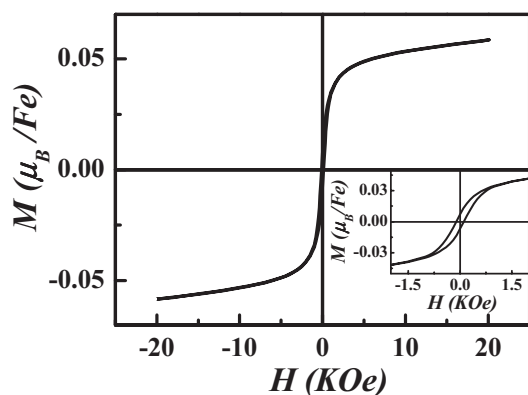


Figure 4. M – H hysteresis loop of the BFO nanoparticles measured at $T = 300 \text{ K}$ (the partially enlarged curve is the inset).

Received: October 19, 2006

Revised: January 23, 2007

Published online: August 28, 2007

-
- [1] Y. P. Wang, L. Zhou, M. F. Zhang, X. Y. Chen, J.-M. Liu, Z. G. Liu, *Appl. Phys. Lett.* **2004**, *84*, 1731.
- [2] C. Tabares-Munoz, J. P. Rivera, A. Monnier, H. Schmid, *Jpn. J. Appl. Phys., Part 1* **1985**, *24*, 1051.
- [3] P. Fischer, M. Polomska, I. Sosnowska, M. Szymanski, *J. Phys. C* **1980**, *13*, 1931.
- [4] K. Takahashi, N. Kida, M. Tonouchi, *Phys. Rev. Lett.* **2006**, *96*, 117402.
- [5] J. Lou, P. A. Maggard, *Adv. Mater.* **2006**, *18*, 514.
- [6] F. Gao, Y. Yuan, K. F. Wang, X. Y. Chen, F. Chen, J.-M. Liu, Z. F. Ren, *Appl. Phys. Lett.* **2006**, *89*, 102506.
- [7] W. Eerenstein, F. D. Morrison, J. Dho, M. G. Blamire, J. F. Scott, N. D. Mathur, *Science* **2005**, *307*, 1203a.
- [8] S. T. Zhang, M. H. Lu, D. Wu, Y. F. Chen, N. B. Ming, *Appl. Phys. Lett.* **2005**, *87*, 262907.
- [9] J. Wang, J. B. Neaton, H. Zheng, V. Nagarajan, S. B. Ogale, B. Liu, D. Viehland, V. Vaithyanathan, D. G. Schlom, U. V. Waghmare, N. A. Spaldin, K. M. Rabe, M. Wuttig, R. Ramesh, *Science* **2003**, *299*, 1719.
- [10] H. Bea, M. Bibes, A. Barthelemy, K. Bouzehouane, E. Jacquet, A. Khodan, J.-P. Contour, S. Fusil, F. Wyczisk, A. Forget, D. Lebeugle, D. Colson, M. Viret, *Appl. Phys. Lett.* **2005**, *87*, 072508.
- [11] D. Wu, Y. F. Chen, J. Liu, X. N. Zhao, A. D. Li, N. B. Ming, *Appl. Phys. Lett.* **2005**, *87*, 112501.
- [12] P. Kubelka, F. Munk, *Tech. Z. Phys.* **1931**, *12*, 593.
- [13] Y. Kim, S. J. Atherton, E. S. Brigham, T. E. Mallouk, *J. Phys. Chem.* **1993**, *97*, 11802.
- [14] G. L. Yuan, S. W. Or, J.-M. Liu, Z. G. Liu, *Appl. Phys. Lett.* **2006**, *89*, 052905.
- [15] A. T. Bell, *Science* **2003**, *299*, 1688.
- [16] R. Asahi, T. Morikawa, T. Ohwaki, K. Aoki, Y. Taga, *Science* **2001**, *293*, 269.
- [17] S. Al-Qaradawi, S. R. Salman, *J. Photochem. Photobiol. A* **2002**, *148*, 161.
- [18] A. V. Zaleskii, A. K. Zvezdin, A. A. Frolov, A. A. Bush, *JETP Lett.* **2000**, *71*, 465.
- [19] C. Ederer, N. A. Spaldin, *Phys. Rev. B* **2005**, *71*, 224103.
-